Songklanakarin J. Sci. Technol.
45 (2), 256–263, Mar. – Apr. 2023

http://www.sjst.psu.ac.th

Original Article

Modeling of the thermal behaviour of reverse thermosyphon, utilizing solar energy and different working fluids

Arjun K. S.[1*], Rakesh Kumar[2], Biju N.[3], and Tide P. S.[3]

[1] *National Engineering School of Gabes, University of Gabes, Gabes, Tunisia*

[2] *Department of Mechanical Engineering, Indian Institute of Technology (ISM), Dhanbad, 826004 India*

[3] *Department of Mechanical Engineering, School of Engineering, Cochin University of Science and Technology, Kochi, Kerala, 682022 India*

Received: 7 August 2021; Revised: 15 October 2022; Accepted: 7 March 2023

Abstract

In solar collectors, the most important challenge is the low performance in off-peak hours of sunlight. Thermal performance of the bubble pump enabled reverse thermosyphon integrated with a U-tube solar collector is evaluated numerically concerning the average temperature along the length of the thermosyphon, thermal resistance, and efficiency. The proposed system is equipped with different nanoparticles and phase change materials at specific concentrations as two working media for passive downward heat transfer. The influences of actual variable heat flux, different fill ratios, and flow rate on thermal processes are analysed along with condensation and evaporation processes of phase change material. The results show a significant enhancement in thermal efficiency of 71% and a high operating temperature up to 98°C. The investigated parameters were found to have a large impact on thermal performance. The best phase change material and the nanoparticle at lower and higher heat flux and the best fill ratio for various heat fluxes are adjudged. Temperature distribution profiles, heat transfer, and thermal performances along with a multi-phase flow visualization of the reverse thermosyphon by CFD simulations are summarised. Quantitative estimation of the performance analysis under the high sink as well as the anti-gravity operating attributes of critical nature is highlighted.

Keywords: thermal efficiency, CFD, anti-gravity, nanofluid, boiling, condensation, evaporation

1. Introduction

Thermal energy recovery and its utilization has improved much by the wide use of two-phase closed thermosyphon systems. Modifications in such devices and consequent temperature profile developments by the geyser and nucleate pool boiling lead to dry-out limit, and expansion of the working fluid (Gallego, Herrera, Sierra, Zapata, & Cacua, 2020). Solar collectors are a practical solution to tap natural energy savings with eco-friendly perspectives. The flammability, limitation of temperature around 400°C, and environmental toxicity are the major disadvantages of using thermal oils (Blanco & Miller, 2017). A potential application of phase changes includes low-temperature heat recovery (Li *et al*., 2020). Sarafraz, Tian, Tlili, Kazi, and Goodarzi (2019) showed that both the fill ratio and the tilt angle were key parameters affecting the system's thermal performance.

Kasaeian, Daneshazarian, Rezaei, Pourfayaz, and Kasaeian (2017) reported augmented heat transfer and maximum thermal efficiency of 30.4% by using 0.3% MWCNT/EG nanofluid. 234% heat transfer coefficient augmentation was reported (Mwesigye, Yılmaz, & Meyer, 2018), using MWCNT/therminol VP-1 nanofluid. A decrease of 20-30% entropy generation, using 6% Cu-Therminol nanofluid (Mwesigye, Huan, & Meyer, 2016) was reported. Optimization of nanoparticle fraction is highly important for hydraulic and thermal performance efficiencies.

*Corresponding author
Email address: arjunks@cusat.ac.in

To achieve a downward passive heat transfer, designing a reverse thermosyphon with self-action and two working media is the best option. In practical applications such devices are not found, due to the need for harmful or costly refrigerants or the requirement of lower pressure in the device than the ambient. Heat-carrying action and pumping action can be performed separately with a second medium having a low boiling point. Introducing fins (Chu, Shen, & Wang, 2021), using the working medium such as methanol (Huang, Lee, Tarau, Kamotani, & Kharangate, 2021) or nanofluid (Wang *et al*., 2020), the influence of boundary conditions (Nguyen & Merzari, 2020), and using an evaporator, smaller than the condenser (Cisterna, Fronza, Cardoso, Milanez, & Mantelli, 2021; Ng, Yu, Wu, & Hung, 2021) increase the thermosyphon thermal efficiency.

Anti-gravity flow movement was 0.38 m with a heat transport of 100 W in a heat pipe loop with porous wick (Tang, Zhou, Lu, & Xie, 2012) and 1 m with 220 W in a 10 m cylindrical heat pipe (Nakamura, Odagiri, & Nagano, 2016). In most anti-gravity passive heat transfer reports, the condenser is kept as the room temperature. This work is conducted with the varying heat flux and anti-gravity conditions available for a solar collector. The temperature along the thermosyphon is studied with the flow rate.

Advancement of dependable and economic means of autonomous heat transfer downwards is not yet tested in the peak annual temperature range. Simultaneous use of two working fluids in a reverse thermosyphon integrated with a bubble pump system, where water transfers heat and a low boiling substance creates pressure above atmospheric pressure and sets water in circulation is a new concept for this solution. Contrary to the thermosyphons that operate cyclically, the proposed system could be distinguished by continuous operation. Outcomes of this study could be used to evaluate the pertinence of reverse thermosyphons in the backdrop of renewable energy generation and play a dominant role in the prosperity of several countries.

2. Materials and Methods

The continuity equations are defined in Fluent (Fluent, 2020) as:

$$\frac{\partial \rho}{\partial t} + \nabla(\rho \vec{v}) = 0 \tag{1}$$

ρ and $\vec{v}$ denotes density and velocity vector.

The momentum equation is:

$$\frac{\partial}{\partial t}(\rho \vec{v}) + \nabla(\rho \vec{v}\vec{v}) = -\nabla \mathrm{p} + \nabla \vec{\tau} + \rho \vec{g} + S_g \tag{2}$$

$\vec{\tau}$ is stress tensor, g is gravity acceleration and p is pressure. The energy equation for phase change (Fluent, 2020) is:

$$\frac{\partial}{\partial x}(\rho H) + \nabla\big(\vec{v}(\rho H + p)\big) = \nabla(k \nabla \mathrm{T} + \vec{\tau}\vec{v}) S_H \tag{3}$$

H is internal energy, *h* is the sum of sensible enthalpy and ΔH is latent heat, and k is thermal conductivity. Sensible enthalpy *h* can be found (Fluent, 2020) below:

$$\Delta H = \beta L \tag{4}$$

β is the liquid fraction of PCM and *L* is the latent heat of PCM. Liquid fraction β is defined by Fluent (2020) as:

$$\beta = 0, if\ T < T_{solidus} \tag{5}$$

$$\beta = 1, if\ T < T_{liquidus} \tag{6}$$

$$\beta = \frac{T - T_{solidus}}{T_{liquidus} - T_{solidus}}, \text{if } T_{solidus} < T < T_{liquidus} \tag{7}$$

$T_{solidus}$ and $T_{liquidus}$ are material temperatures at solid and liquid phases and the temperature of the PCM is denoted by T.

The equation for the stress tensor $\vec{\tau}$ is as follows (Fluent, 2020):

$$\vec{\tau} = \mu\left[(\nabla \vec{v} + \nabla \vec{v}^T) - \frac{2}{3}\nabla \cdot \vec{v} I\right] \tag{8}$$

I is unit tensor and μ is molecular viscosity. For natural convection and mushy region, source term S_g was considered as follows (Pawar & Sobhansarbandi, 2020):

$$S_g = \rho \vec{g} \beta\big(T - T_{ref}\big) - \frac{(1-\beta)^2}{\beta^3 + \epsilon} A_{mushy} \vec{v} \tag{9}$$

The second term in equation 9 relates to the porosity of medium in each cell where liquid fraction is considered (Pawar & Sobhansarbandi, 2020). A_{mushy} is mushy zone constant (mushy zone is mixed solid-liquid region) set at 100,000. To avoid a division by zero, ϵ was set at 0.001 (Fluent, 2020).

Heat removal factor (F_R) is the ratio of actual heat transfer to maximum heat transfer. The Hottel–Whillier–Bliss (Bliss, 1959; Hottel & Whillier, 1958; Whillier, 1967) equations were used to evaluate the instantaneous thermal efficiency (η_{th}), using a modified efficiency curve model. The absorbed radiation is the product of the incident radiation and the transmittance-absorptance product (τ_α).

Relationship of absorptance of the absorber (α) cover transmittance (τ), overall heat transfer coefficient (U_L, W/m^{2}K), inlet fluid temperature (T_i, *K*), ambient temperature (T_a, *K*) and global solar radiation (G_T, W/m^2) are given as follows (Duffie & Beckman, 2013):

$$\eta_{th} = \frac{Q}{A_c G_T} = \frac{\dot{m} C_p (T_0 - T_i)}{G_T} \tag{10}$$

Q is the rate of solar energy gained (W), $\dot{m}$ is the fluid flow rate (l/hr), C_p is heat capacity (J/kgK), T_i, T_a and T_0 are temperatures (K) of the inlet, ambient, and outlet respectively, A_c is surface area (m^2).

$$\eta_{th} = F_R \tau_\alpha - F_R U_L \frac{(T_i - T_a)}{G_T} \tag{11}$$

Nanofluid closed circulation is maintained by keeping the evaporator with a tilt angle of 65°. Fluid inlet, surface, ambient, and outlet temperatures, friction factor, wind velocity, and global solar radiation are found. The flow rates of nanofluids are varied for the study. The Reynolds number in the collector ($Re = 4\dot{m}/\pi d\mu$) of nanofluid with the viscosity (μ) is calculated by the tube hydraulic diameter/inner diameter (d).

Increased resistance of fluid causes pressure drop. The friction factor is:

$$f = \frac{\Delta P}{\left(\frac{l}{d}\right)\left(\frac{\rho V^2}{2}\right)} \tag{12}$$

l is tube length (mm), ΔP is pressure drop, v is velocity, and ρ is density.

Nusselt number is:

$$Nu = \frac{hd}{k} \tag{13}$$

Heat transfer coefficient (W/m^2K) $h = Q/A_c(T_s - T_b)$, T_s is outlet fluid temperature after time t, T_b is arithmetic average of outlet and inlet temperatures, k is the thermal conductivity (W/mK). $A_c = \pi dL, T_s = T_1 + T_2 + T_3/3$ and $T_b = T_o + T_i/2$.

Transmittance for visible wavelength and absorptance of the plate are $\tau = 0.89$ and $\alpha = 0.89$.

The thermal resistance of the evaporator R_e (°C/W) is:

$$R_e = \frac{T_{ew} - T_{ev}}{Q_e} \tag{14}$$

T_{ew} is wall temperature, T_{ev} is vapor temperature and Q_e is input power. Condenser thermal resistance (R_c) is:

$$R_c = \frac{T_{cv} - T_{cw}}{Q_e} \tag{15}$$

T_{cw} is wall temperature of condenser, Q_e is input power and T_{cv} is vapor temperature. Total thermal resistance (R) of the heat pipe is (Mousa, 2011):

$$R = \frac{T_{ew} - T_{cw}}{Q_e} \tag{16}$$

Heat transfer coefficient at the evaporator h_e (W/m^2K) is:

$$h_e = \frac{Q}{A(T_{ew} - T_e)} \tag{17}$$

The simulation performance of thermosyphon is illustrated by thermal resistance on an overall basis.

Heat transfer rate Q on an overall basis is:

$$Q = \frac{T_e - T_c}{R_{eq}} \tag{18}$$

where T_e and T_c are evaporator and condenser average wall temperatures, R is thermal resistance (K/W) and Q is power throughput.

The filling ratio FR is:

$$FR = \frac{V_l}{Al_e} \times 100 \tag{19}$$

A is the internal cross-section area, l_e is the length of an evaporator, and V_l is liquid volume.

3. CFD Modeling

A pressure-based solver, a SIMPLE algorithm with PRESTO!, least-square cell-based method, and second-order upwind mode were used. The evaporator section is indicated by the distance between 0 and 200 mm, the distance between 300 and 500 mm indicates the condenser section and the middle section is the adiabatic region. A UDF code is used for creating a closed-loop piping system and another UDF for the phase change process.

The simulation was conducted with a constant heat flux of a solar thermal collector, placing the thermosyphon above it. Reverse thermosyphon having two working media (Figure 1) consist of a U-tube (U) with a fin (F) of the solar thermal collector providing heat flux, bubble pump (B), an evaporator (E), a separator (S), and a condenser (C); which are interconnected to become a closed system for the liquid. The evaporator is partly filled with a liquid medium (LM) of heat transfer and pumping medium (PM). A film of the pumping medium of 9-10 mm on the bulk of the liquid medium is introduced as a layer. Liquid medium shows maximum flow rate during slug flow (Hanafizadeh, Karimi, & Saidi, 2011) in a two-phase study of a bubble pump.

Stagnation (on-demand) operation was used for preliminary simulation with no circulation of HTF throughout the system till achieving maximum energy storage and circulation of HTF is initiated in the system at a later time of the day (Papadimitratos, Sobhansarbandi, Pozdin, Zakhidov, & Hassanipour, 2016). This is a new system of study with no prior experimental work or data.

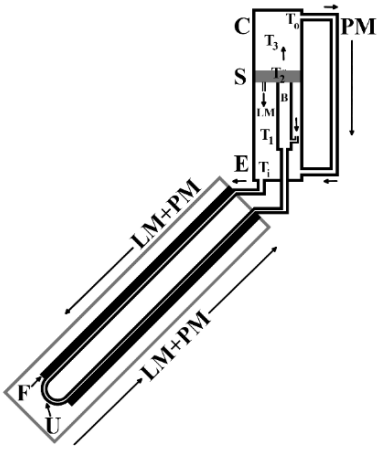

Figure 1. Circuit diagram of bubble pump enabled reverse thermosyphon with two working media.

4. Mesh Geometry and Independence

GAMBIT software was used to generate two-dimensional geometry and meshing. The first grid size was 0.01 mm and the growth ratio was 1.2. 36 cells constituting one cell layer are set apart for top and lower walls since heat conduction does not take place through these. Grid-independence results for the reverse thermosyphon charged with water for heat input of 100 W for a mesh size of 19,500 (cells) shows that the evaporator, separator, and condenser registered mean temperatures of 30.51, 26.03, and 21.48°C respectively and those with a mesh size of 69,276 were 29.16, 25.86 and 22.45°C respectively; and those for a mesh size of 129,944 were 29.32, 25.89 and 22.47 respectively. Thus, the mesh size selected for the numerical study was 69,276. The solid region contains 15,092 cells and 54,184 quad cells for the fluid region. As a result, 69,276 cells are generated. Fifteen cell layers are selected to analyse the film of liquid getting developed near the left and right wall regions. The mesh sizes of 69,276 and 129,944 revealed very similar values of mean temperature for evaporator, separator, and condenser.

5. Initial and Boundary Conditions

- Constant heat flux at evaporator wall with no slip at inner walls.
- Zero heat flux at upper and lower ends as well as a separator.
- Convection heat transfer with heat transfer coefficient values from the CFD simulation of the condenser at the walls of the condenser.
- Interfaces between solid and fluid regions of the heat pipe are assumed as the coupled wall.
- Physical properties at 298.15 K are assumed temperature independent; except for density and surface tension of liquid phase.

6. Validation

As shown in Figure 2, as the heat flux increases from 100.41 to 376.14W/m^2, the temperature between evaporator and condenser in computational results were compared to experimental work (Fadhl, Wrobel, & Jouhara, 2013) and it was observed that the temperature increases, and the thermal resistance decreases. The average deviation percentage for temperature between evaporator and condenser experimentally and computationally was 3.7 %. For temperature between evaporator and condenser, the highest deviation between experiment and computation was observed at a heat flux of 100.41W/m^2, the deviation after that at a heat flux of 172.87W/m^2 to 376.14W/m^2 was 14 %. In the experiment, only two thermocouple positions were used to record the average temperature of the evaporator section (Fadhl, Wrobel, & Jouhara, 2013) and this might be the reason for the large deviation at a low heat flux. Therefore, excluding the lowest heat flux of 100.41W/m^2, the computational results obtained for temperature are extremely close to the experimental values for temperature between evaporator and condenser. In the case of heat inputs beyond 170 W, the thermal resistance is relatively independent of the heat input (Fadhl, Wrobel, & Jouhara, 2013). In the case of lower heat inputs, the thermal resistance tends to increase. In CFD software, the ideal adiabatic condition was considered and so the deviation was obtained while comparing both the results.

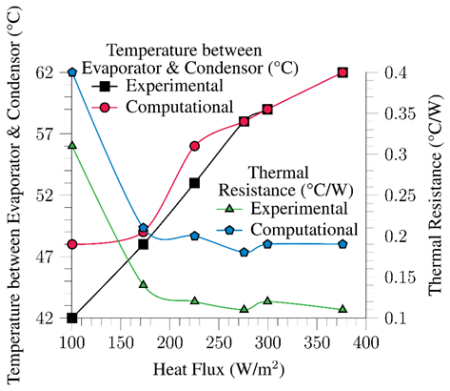

Figure 2. Validation of computational results

7. Results

Figure 3 depicts the distribution of temperature on the thermosyphon surface and when ammonia is used, the stability of the distribution of temperature became lower than in case of using water. The flow rate was kept as 10 l/h with a filling ratio of 60%. Water that has a higher evaporation temperature than ammonia might be the major cause of this behaviour. The flow rate of cooling water gets improved, though the distribution of temperature at the evaporator surface gets decreased from that with water. When we use ammonia, the reverse effect is noticed. Using ethylene glycol having better heat transfer capacity, the stability of temperature distribution and mean surface temperatures of condenser and evaporator are higher. The melting and freezing onset difference of roughly $30\,°C$ makes Erythritol a strong candidate as an HTF due to Erythritol's ability to stay in liquid form for a longer period to prevent thermal expansion from crystallizing and transferring heat for a longer period.

Ethylene glycol showed an efficiency of 89% for the 200W heat input. The efficiency observed was 37.8 % for the 500 W heat input (Figure 4). As the heat input increases, the thermal efficiency decreases. Though Erythritol showed less thermal efficiency than ethylene glycol and ammonia, it showed the highest thermal efficiency of 37.8 % at 500 W heat input. As the average real heat input is higher than 200 W most times, Erythritol is adjudged as a better PCM in thermosyphon with variable heat input from U-tube solar collector. Using phase change materials, by increasing heat input, thermal efficiency is lowered as the very high latent heat will be turned to superheated steam.

The highest thermal efficiency in Figure 5 is 58% at 500 W heat input for 0.2 % Ag. The thermal efficiency of 0.2 % Ag (29.6 %) is much lower at lower heat input but it becomes the highest at high heat input. The thermal efficiency of the nanofluid increases with an increase in heat input from 200 W to 500 W. The thermal efficiency observed for 0.2 % MWCNT is 52 % at 500 W heat input and the thermal efficiency observed for 200 W is 38 %. The thermal efficiency at 200 W is higher than that of 0.2 % Ag. Hence, the Ag nanoparticles show better thermal efficiency at a higher heat input and the MWCNT nanoparticles shows better thermal efficiency at a lower heat

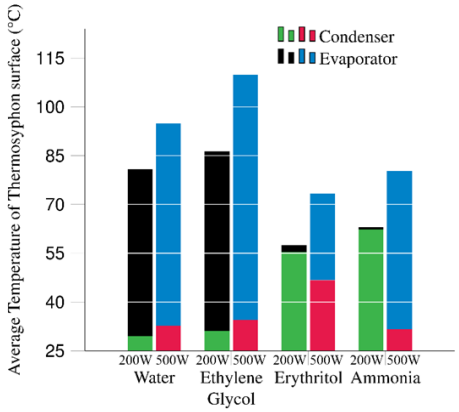

Figure 3. Average temperature of thermosyphon surface using PCM

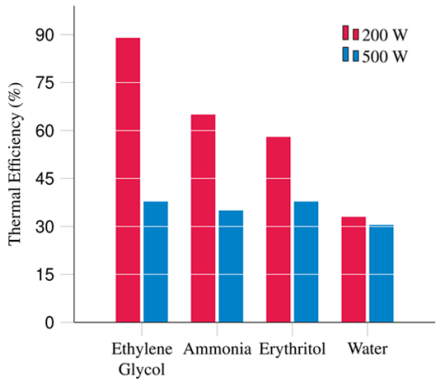

Figure 4. Thermal efficiency of PCM in thermosyphon

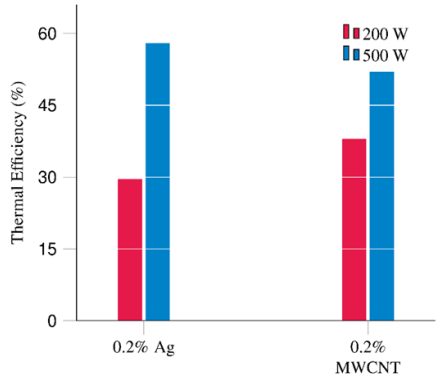

Figure 5. Thermal efficiency of thermosyphon using different nanoparticles

input. Using nanofluid materials, by increasing heat input, thermal efficiency also is enhanced.

In Figure 6, it is observed that the thermal resistance decreases as heat flux increases from 100 to 500 W/m^2. The average thermal resistance is 0.37 for 100 W/m^2 and 0.07 for 500 W/m^2 on using Erythritol. Similar trends have been reported earlier (Solomon, Roshan, Vincent, Karthikeyan, & Asirvatham, 2015; Sözen *et al*., 2016). Thermal resistance decreases with heat flux non-linearly as the heat transfer mechanism changes to nucleate boiling from convection.

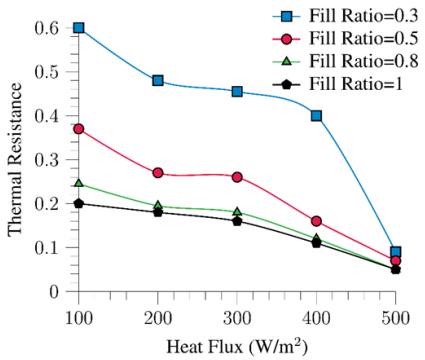

Figure 6. Thermal resistance in thermosyphon using Erythritol as PCM

Identical results of thermal efficiency improvement of 95.94 - 137.07 % were seen on using ethylene glycol, and upon changing the flow rate to 30 l/h from 10 l/h (Figure 7), compared to water. Similar behaviour is noticed at almost all the heat inputs investigated in this study. Hence, the thermal efficiency elevation or reduction depends on the flow rate. Karthikeyan, Vaidyanathan, and Sivaraman, (2010) reported an increase, and Sözen *et al*., (2016) reported a reduction in thermal efficiency with the flow rate. The reduction of thermal efficiency from increased flow rate might be due to the flow reversal at the outlet, which reduced both the flow rate and its temperature rise.

As the heat input increases from 100 to 500 W, the difference in temperature between the evaporator and the condenser increases (Figure 8). The average temperature of evaporator and condenser is 83.02°C for ethylene glycol and 48.52 °C for ammonia. The average temperature of the evaporator of the thermosyphon on using ethylene glycol as the PCM was 122.25°C.

When ammonia and ethylene glycol are used as PCM in working fluid water with a flow rate of 10 l/h and 200 W heat input, the mean difference in temperature was 12.9 °C for ethylene glycol and 11.3 °C for ammonia. When the heat input was changed to 500 W, these values were 16.57 °C and 22.9 °C respectively (Figure 8). When the flow rate was changed to 30 l/h, these values were 17.5 °C and 4.7 °C respectively with 200 W. When the flow rates were similar, a rise in heat input makes the differences in temperature higher, and when the flow rate rises, the temperature differences get lowered concerning the working fluids investigated (Sözen *et al*., 2016). Ethylene glycol was found to be a better PCM at a lower heat input and ammonia was found to be a better PCM at a higher heat input.

As shown in Figure 9 as the heat flux increases from 100 to 500 W/m^2, the temperature of evaporator and condenser increases with a very high rate of increase from 100 to 200 W/m^2. The average difference in temperature is 68°C for 0.2% MWCNT with Erythritol as the PCM is highest for fill ratio 0.8 with 500 W/m^2 heat flux. As the fill ratio increases from 0.3 to 0.8, the temperatures of evaporator and condenser increase. The thermal efficiency has registered a maximum of 70.5 % for fill ratio 0.5 with 500 W/m^2 heat flux. Even though the fill ratio of 0.8 showed a thermal efficiency on par with a fill ratio of 0.5 from 100 to 250 W/m^2 heat flux, it showed a lesser thermal efficiency after 250 W/m^2 heat flux input. Thermal efficiency increases with an increase in heat flux.

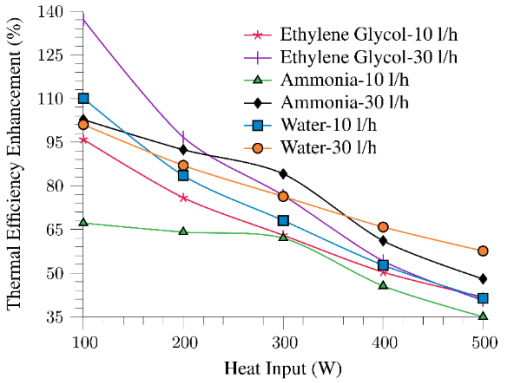

Figure 7. Thermal efficiency enhancement in thermosyphon using different PCM and flow rates

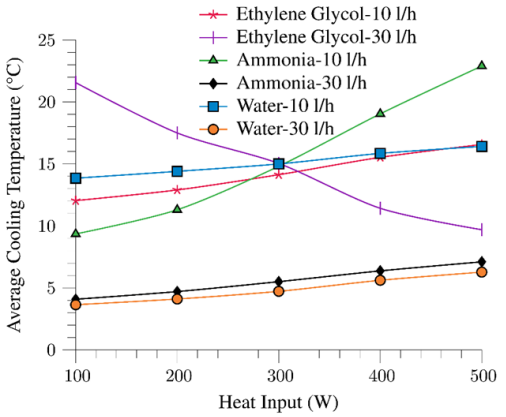

Figure 8. Average cooling temperature of thermosyphon using different PCMs and flow rates

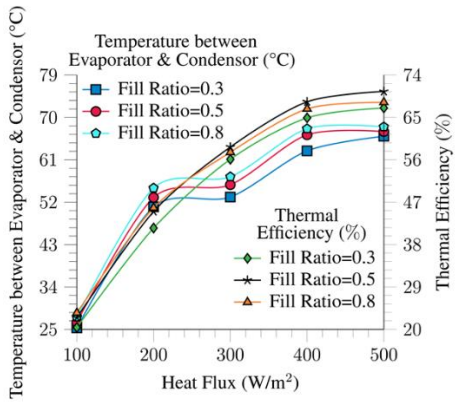

Figure 9. Thermal efficiency and difference in temperature in thermosiphon

The temperature profile from the start of the evaporator (Es) at 20 mm length of thermosyphon to the end of the condenser (Ce) using 0.2% MWCNT and Erythritol as PCM with heat input of 100-500 W, is shown in Figure 10. The temperature increases as heat input increases in the evaporator with the highest value of 97.99 $°C$ for 500 W at 170 mm length (end of the evaporator, Ee). The adiabatic section also shows a decrease in temperature from its start (As) to end (Ae) for the lower heat input, whereas a slight increase is registered with the higher heat inputs from 220-270 mm length. A similar trend is observed in the condenser for all the heat inputs, whereas a slight increase is observed with 200 W from 350-450 mm length. The lowest condenser temperatures, 50.49 $°C$ for 500 W, and 30.5 $°C$ for 100 W were noted. The whole length of the thermosyphon has shown a temperature variation of 20-42$°C$.

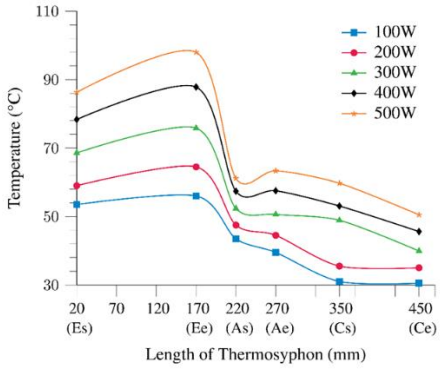

Figure 10. Surface temperature of thermosyphon on using nanoparticles and PCM

8. Conclusions

The present study used a combination of heat transfer and storage in a single unit, in which the U-tube effectively replaces the thermosyphon heat pipe. A simple condenser section is created by extending one side of the U-tube geometry where the heat transfer fluid in the U-tube transfers heat to water, as if in a simple heat exchanger configuration.

Erythritol is adjudged as a better PCM in bubble pump enabled reverse thermosyphon with variable heat flux from U-tube solar collector, than ethylene glycol and ammonia, concerning the average temperature of thermosyphon surface. Ag nanoparticles show better thermal efficiency at a higher heat flux and MWCNT nanoparticles show a better thermal efficiency at a lower heat flux, at a concentration of 0.2%. With the flow rate, the thermal efficiency tends to either decrease or increase. For ethylene glycol the efficiency decreases with flow rate, but for water and ammonia it increases. The reduction of the thermal efficiency consequent on flow rate increase might be due to a flow reversal at the outlet, which reduces both the flow rate and the temperature rise. Ethylene glycol was found to be a better PCM at a lower heat flux and ammonia was found to be a better PCM at a higher heat flux, compared to water, concerning the cooling temperature.

References

Blanco, M. J., & Miller, S. (2017). Introduction to concentrating solar thermal (CST) technologies. *Advances in Concentrating Solar Thermal Research and Technology* (pp. 3-25). Amsterdam, Netherlands: Elsevier. doi:10.1016/B978-0-08-100516-3.00001-0

Bliss, R. W. (1959). The derivation of several plate efficiency factors useful in the design of flat plate solar heat collectors. *Solar Energy, 3*(*4*), 55–64. doi: 10.1016/0038-092X(59)90006-4

Chu, W. X., Shen, Y. W., & Wang, C. C. (2021). Enhancement on heat transfer of a passive heat sink with closed thermosyphon loop. *Applied Thermal Engineering*, *183*(*2*), 116243. doi:10.1016/j.applthermaleng.2020.116243

Cisterna, L. H., Fronza, E. L., Cardoso, M. C., Milanez, F. H., & Mantelli, M. B. (2021). Modified biot number models for startup and continuum limits of high temperature thermosyphons. *International Journal of Heat and Mass Transfer*, *165*(*B*), 120699. doi:10.1016/j.ijheatmasstransfer.2020.120699

Duffie, J. A., & Beckman, W. A. (2013). *Solar engineering of thermal processes* (4th ed.). Hoboken, NJ: John Wiley and Sons. doi:10.1002/9781118671603

Fadhl, B., Wrobel, L. C., & Jouhara, H. (2013). Numerical modelling of the temperature distribution in a two-phase closed thermosyphon. *Applied Thermal Engineering*, *60*(*1*), 122–131. doi:10.1016/j.applthermaleng.2013.06.044

Fluent, A. (2020). *ANSYS FLUENT 2020 R1 -Theory guide; User's guide*. Canonsburg, PA, ANSYS Incorporated.

Gallego, A., Herrera, B., Sierra, R. B., Zapata, C. & Cacua, K. (2020). Influence of filling ratio on the thermal performance and efficiency of a thermosyphon operating with Al_2O_3-water based nanofluids. *Nano-Structures and Nano-Objects*, *22*, (100448), 1-10. doi:10.1016/j.nanoso.2020.100448

Hanafizadeh, P., Karimi, A., & Saidi, M. H. (2011). Effect of step geometry on the performance of the airlift pump. *International Journal of Fluid Mechanics Research*, *38*(*5*), 387-408. doi:10.1615/InterJFluidMechRes.v38.i5.10

Hottel, H. C., & Whillier, A. (1958). Evaluation of flat plate collector performance, *Transmission Conference on the Use of Solar Energy*, *2*(*1*), 74-104.

Huang, C. N., Lee, K. L., Tarau, C., Kamotani, Y., & Kharangate, C. R. (2021). Computational fluid dynamics model for a variable conductance thermosyphon. *Case Studies in Thermal Engineering*, *25*, 100960. doi:10.1016/j.csite.2021.100960

Karthikeyan, M., Vaidyanathan, S., & Sivaraman, B. (2010). Thermal performance of a two phase closed thermosyphon using aqueous solution, *International Journal of Engineering Science and Technology*, *2*(*5*), 913–918. doi:10.1.1.165.5741

Kasaeian, A., Daneshazarian, R., Rezaei, R., Pourfayaz, F., & Kasaeian, G. (2017). Experimental investigation on the thermal behavior of nanofluid direct absorption in a trough collector. *Journal of Cleaner Production*, *158*, 276-284. doi:10.1016/j.jclepro.2017.04.131

Li, Z., Sarafraz, M. M., Mazinani, A., Moria, H., Tlili, I., Alkanhal, T.A., Goodarzi, M., & Safaei, M. R. (2020). Operation analysis, response and performance evaluation of a pulsating heat pipe for low temperature heat recovery. *Energy Conversion and Management*, *222*, 113230. doi:10.1016/j.enconman.2020.113230

Mousa, M. G. (2011). Effect of nanofluid concentration on the performance of circular heat pipe. *Ain Shams Engineering Journal*, *2*, 63–69. doi:10.1016/j.asej.2011.03.003

Mwesigye, A., Huan, Z., & Meyer, J. P. (2016). Thermal performance and entropy generation analysis of a high concentration ratio parabolic trough solar collector with Cu-Therminol® VP-1 Nanofluid. *Energy Conversion Management*, *120*, 449-465.doi:10.1016/j.enconman.2016.04.106

Mwesigye, A., Yılmaz, I. H., & Meyer, J. P. (2018). Numerical analysis of the thermal and thermodynamic performance of a parabolic trough solar collector using SWCNTS-Therminol® VP-1 nanofluid. *Renewable Energy*, *119*, 844-862. doi:10.1016/j.renene.2017.10.047

Nakamura, K., Odagiri, K., & Nagano, H. (2016). Study on a loop heat pipe for a long-distance heat transport anti-gravity condition. *Applied Thermal Engineering*, *107*, 167–174. doi:10.1016/j.applthermaleng.2016.06.162

Ng, V. O., Yu, H., Wu, H. A., & Hung, Y. M. (2021). Thermal performance enhancement and optimization of two-phase closed thermosyphon with graphene-nanoplatelets coatings. *Energy Conversion and Management*, *236*, 114039. doi:10.1016/j.enconman.2021.114039

Nguyen, T., & Merzari, E. (2020). Computational fluid dynamics simulation of a single-phase rectangular thermosyphon. *Proceedings of the International Conference on Nuclear Engineering*, *3*. American Society of Mechanical Engineers Digital Collection, Anaheim, CA. doi: 10.1115/ICONE2020-16934

Papadimitratos, A., Sobhansarbandi, S., Pozdin, V., Zakhidov, A., & Hassanipour, F. (2016). Evacuated tube solar collectors integrated with phase change materials. *Solar Energy*, *129*, 10 – 19. doi:10.1016/j.solener.2015.12.040

Pawar, V. R., & Sobhansarbandi, S. (2020). CFD modeling of a thermal energy storage based heat pipe evacuated tube solar collector. *Journal of Energy Storage*, *30*, 101528. doi:10.1016/j.est.2020.101528

Sarafraz, M. M., Tian, Z., Tlili, I., Kazi, S., & Goodarzi, M. (2019). Thermal evaluation of a heat pipe working with n-pentane-acetone and n-pentane-methanol binary mixtures. *Journal of Thermal Analysis and Calorimetry*, *139* (*4*), 2435–2445. doi:10.1007/s10973-019-08414-2

Solomon, A. B., Roshan, R., Vincent, W., Karthikeyan, V. K., & Asirvatham, L. G. (2015). Heat transfer performance of an anodized two-phase closed thermosyphon with refrigerant as working fluid, *International Journal of Heat and Mass Transfer*, *82*, 521–529. doi:10.1.1.165.5741

Sözen, A., Menlik, T., Gürü, M., Boran, K., Kılıc, F., Aktas, M., & ÇAkır, M.T. (2016). A comparative investigation on the effect of fly-ash and alumina nanofluids on the thermal performance of two-phase closed thermo-syphon heat pipes. *Applied Thermal Engineering*, *96*, 330–337. doi:10.1016/j.applthermaleng.2015.11.038

Tang, Y., Zhou, R., Lu, L., & Xie, Z. (2012). Anti-gravity loop-shaped heat pipe with graded pore-size wick. *Applied*

Thermal Engineering, *36*, 78–86. doi:10.1016/j.applthermaleng.2011.12.026

Wang, W. W., Cai, Y., Wang, L., Liu, C. W., Zhao, F. Y., Sheremet, M. A., & Liu, D. (2020). A two-phase closed thermosyphon operated with nanofluids for solar energy collectors: Thermodynamic modeling and entropy generation analysis. *Solar Energy*, *211*, 192–209. doi:10.1016/j.solener.2020.09.031

Whillier, A. (1967). *Design factors influencing collector performance*. *Low temperature engineering application of solar energy*. New York, NY: ASHRAE